2017

Extended Protein Ions are Formed by the Chain Ejection Model in Chemical Supercharging Electrospray Ionization

Micah T. Donor

Simon A. Ewing

Muhammad A. Zenaidee

William A. Donald

James S. Prell

Extended Protein Ions Are Formed by the Chain Ejection Model in Chemical Supercharging Electrospray Ionization

Micah T. Donor,[†] Simon A. Ewing,[†] Muhammad A. Zenaidee,[‡] William A. Donald,[‡] and James S. Prell*[,†,§]

[†]Department of Chemistry and Biochemistry, University of Oregon, Eugene, Oregon 97403-1253, United States

[‡]School of Chemistry, University of New South Wales, Sydney, New South Wales 2052, Australia

[§]Materials Science Institute, University of Oregon, Eugene, Oregon 97403-1252, United States

ABSTRACT: Supercharging electrospray ionization can be a powerful tool for increasing charge states in mass spectra and generating unfolded ion structures, yet key details of its mechanism remain unclear. The structures of highly extended protein ions and the mechanism of supercharging were investigated using ion mobility-mass spectrometry. Head-to-tail-linked polyubiquitins (Ubq_{1-11}) were used to determine size and charge state scaling laws for unfolded protein ions formed by supercharging while eliminating amino acid composition as a potential confounding factor. Collisional cross section was found to scale linearly with mass for these ions and several other monomeric proteins, and the maximum observed charge state for each analyte scales with mass in agreement with an analytical charge state scaling law for protein ions with highly extended structures that is supported by experimental gas-phase basicities. These results indicate that these highly unfolded ions can be considered quasi-one-dimensional, and collisional cross sections modeled with the Trajectory Method in Collidoscope show that these ions are significantly more extended than linear α-helices but less extended than straight chains. The effect of internal disulfide bonds on the extent of supercharging was probed using bovine serum albumin, β-lactoglobulin, and lysozyme, each of which contains multiple internal disulfide bonds. Reduction of the disulfide bonds led to a marked increase in charge state upon supercharging without significantly altering folding in solution. This evidence supports a supercharging mechanism in which these proteins unfold before or during evaporation of the electrospray droplet and ionization occurs by the Chain Ejection Model.

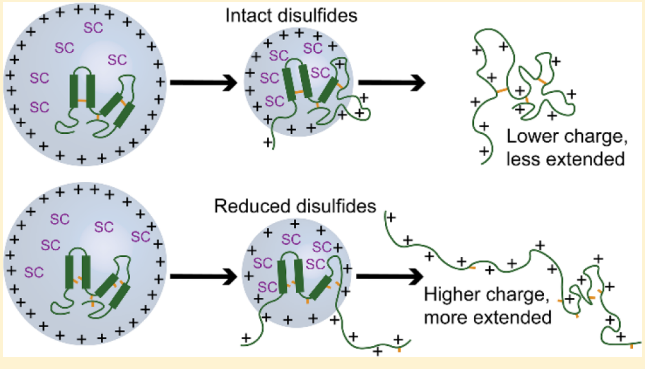

Electrospray ionization (ESI) can be used to ionize folded proteins from buffered aqueous solutions at or near physiological pH values while retaining noncovalent interactions and high-order structure.[1,2] Mass spectrometry (MS) can often be used to determine properties such as complex stoichiometry,[3−5] the number and chemical identity of bound ligands,[6−9] and, when coupled with ion mobility spectrometry (IM-MS), the overall size and shape of the protein ions or complexes determined from collisional cross section (CCS) measurements.[10−12] In contrast to other common ionization methods, such as MALDI, ESI of proteins produces a set of multiply charged ions with a distribution of intensities (charge state envelope). Furthermore, folded protein ions formed by conventional ESI typically populate relatively low charge states, while denatured proteins exhibit higher charge states. The ability to manipulate protein charge states can also be useful. For example, higher charge states can improve mass accuracy in high-resolution MS and lead to greater fragmentation efficiency in electron capture or transfer dissociation or collision-induced dissociation (CID),[13−15] and compact protein ions with lower charge states can be more resistant to gas-phase unfolding due to activation, including in surface-induced dissociation (SID) experiments used to infer oligomer structure.[16−19] Solution additives to either raise or lower charge states have been found: "supercharging" reagents often increase observed charge states,[20−23] while charge reduction reagents tend to decrease charge states and are routinely used to limit unfolding of protein complexes prior to dissociation, as in SID experiments.[18,19,24−26] Supercharging can alternatively be accomplished by raising the nanoESI spray potential (electrothermal supercharging).[27]

Multiple mechanisms have been proposed to explain charging in ESI under native and denaturing conditions. In the ion evaporation model (IEM),[28] charged species are emitted from nanometer-sized droplets. By contrast, in the charged residue model (CRM),[29] the solvent droplet fully evaporates and the residual charges are transferred to the

analyte(s) inside the droplet, with the number of charges roughly corresponding to the Rayleigh-limit charge (the charge at which the Coulomb repulsion balances with the solvent surface tension) of an equivalently sized solvent droplet. In the chain ejection model (CEM),[30,31] a disordered (bio)polymer chain is partially ejected from the droplet, leading to proton migration to the exposed portion of the ion, followed by further extrusion and ultimate ejection of the extended chain. The CEM was proposed to explain the high charge states observed in mass spectra of proteins electrosprayed from denaturing solutions. Much current evidence suggests that folded proteins formed by ESI from buffered aqueous solution ionize by the CRM, small ions by the IEM, and unfolded, disordered proteins by the CEM.[32−34] The CRM predicts that charge state is roughly proportional to ion surface area for quasi-spherical ions and thus the charge state should scale as approximately the square root of mass. Similarly, the CCS of a quasi-spherical ion of fixed density should scale approximately as the two-thirds power of its mass. Experimental CCS data for a variety of native-like protein ions follows the two-thirds power law,[35−37] while the experimental scaling power for average charge state is slightly greater than one-half (0.54−0.57).[32,38−43] These results provide additional support for the CRM and demonstrate the efficacy of inferring structural and mechanistic details based on scaling laws. For highly charged, unfolded protein ions that likely adopt coil-like and extended conformations in the gas-phase, scaling laws for CCS and charge are difficult to predict a priori, although empirical scaling laws for similarly sized intrinsically disordered protein ions have been found experimentally.[38,39] Simultaneous determination of experimental charge state and CCS scaling laws with comparison to theoretical models will improve understanding of the structures of unfolded protein ions and may enable more precise determination of ion structure than either charge state or CCS alone.

Manipulating charge states via conventional, that is, chemical, supercharging is typically accomplished by adding small amounts (1−5%) of polar, high-boiling point compounds such as *m*-nitrobenzyl alcohol (*m*-NBA) or sulfolane to ESI samples. (Hereafter, we use the term "supercharging" to refer to chemical, as opposed to electrothermal, supercharging.) Recently, 1,2-butylene carbonate (BC) and other alkyl carbonates have been shown in some cases to be more effective supercharging reagents than *m*-NBA or sulfolane.[44−46] The magnitude of the observed charge state increase can vary from a few percent[22,47] to a 2-fold increase,[45,46] depending on solution conditions and the chemical identity of the supercharging reagent. In addition to increasing charge states, supercharging has been used to reduce salt adduction to proteins,[48] and as a way to bypass a solution-phase acidic quench step in top-down hydrogen/deuterium exchange experiments.[49]

Many details of the mechanism of supercharging remain poorly understood, although multiple mechanisms for supercharging have been proposed.[21,47,50−53] The quantities of supercharging reagents used will have only minor effects on protein structure in bulk solution. It has been hypothesized that chemical and/or thermal denaturation in the droplet during the late stages of ESI is responsible for supercharging.[21,47,50,51] Recently, Konermann has proposed a mechanism whereby enrichment of the droplets in the supercharging reagent leads to charges becoming trapped on the surface of the folded protein, which after solvent evaporation unfolds due to Coulomb repulsion of the charge sites.[52] This mechanism is supported by molecular dynamics simulations using force fields optimized for bulk solution and in which sodium ions are the charge source. Understanding the mechanism of supercharging, including estimating the time scale of protein unfolding and the chemical environment in which it occurs, is of both fundamental and practical importance.

In order to elucidate the mechanism of supercharging, we show that the effects of supercharging do not depend strongly on protein size or amino acid composition for a variety of monomeric protein ions with masses up to 94 kDa, that largely folded structures are retained in bulk supercharging solution, and that similar starting structures can lead to dramatically different ion charge states and CCSs for protein ions with native and reduced internal disulfide bonds. We derive a simple analytical model that predicts the extent of charging for highly extended protein ions and accurately reproduces the experimental observations. CD data confirm that supercharging reagents minimally perturb protein structure in bulk solution, while internal disulfide reduction leads to an increase in the extent of protein charging, suggesting that supercharging causes these proteins to unfold within the ESI droplet prior to ejection and proceeds via a CEM-like ionization mechanism rather than a CRM-like mechanism.

METHODS

Sample Preparation. Head-to-tail-linear Ubq_{2-11} were purchased from Enzo Life Sciences, the 31-kDa N-terminal domain of anthrax lethal factor protein (LF_N) and anthrax protective antigen (PA_{63}) were graciously provided by Dr. Bryan Krantz (University of Maryland), and bovine serum albumin (BSA), lysozyme, cytochrome C, ubiquitin, myoglobin (Mg), avidin, concanavalin A, carbonic anhydrase (CA), alcohol dehydrogenase (ADH), and β-lactoglobulin were purchased from Sigma-Aldrich. Lyophilized proteins were reconstituted in ultrapure (18 MΩ) water. In experiments with reduced BSA, β-lactoglobulin, and lysozyme, the protein was incubated with 50 mM dithiothreitol for 2 h at 37 °C (BSA), 18 h at 37 °C (β-lactoglobulin), or 18 h at ambient temperature (lysozyme) to reduce the internal disulfide bonds. CD or mass spectral analysis of reduced bovine serum albumin, β-lactoglobulin, or lysozyme was performed immediately following reduction to limit re-formation of disulfide bonds. For native IM-MS experiments, protein samples were buffer-exchanged using Micro Bio-Spin 6 columns (Bio-Rad) into either 200 mM ammonium acetate/10 mM ammonium bicarbonate at pH 7.0 (LF_N and PA_{63}) or 200 mM ammonium acetate at pH 7.2 (all other proteins) with a protein concentration of 1−10 μM. For denaturing experiments, protein samples were buffer-exchanged using Micro Bio-Spin 6 columns into 49/49/2 v/v/v water/methanol/acetic acid at a protein concentration of 1−10 μM. For supercharging experiments, protein samples were buffer-exchanged using Micro Bio-Spin 6 columns into 94.5/5/0.5 v/v/v water/1,2-butylene carbonate (BC)/acetic acid at a protein concentration of 1−10 μM. Samples for circular dichroism spectroscopy were prepared using either pure water, 49/49/2 v/v/v water/methanol/acetic acid (denaturing conditions), or 94.5/5/0.5 v/v/v water/BC/acetic acid (supercharging conditions) at a protein concentration of approximately 5 μM.

Mass Spectrometry. Ion mobility-mass spectra were acquired at the University of Oregon using a Synapt G2-*Si* ion mobility-mass spectrometer (Waters Corp.) equipped with a nanoelectrospray (nanoESI) source. NanoESI emitters with a

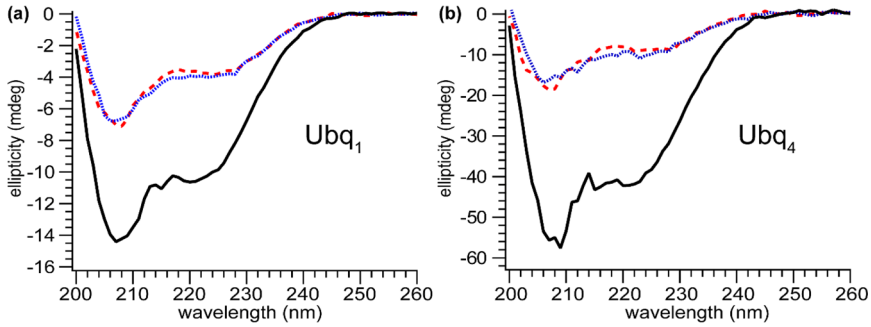

Figure 1. Circular dichroism spectra of (a) Ubq_1 and (b) Ubq_4 in water (dashed red line), supercharging conditions (dotted blue line), and denaturing conditions (solid black line).

tip ID of less than 1 μm were pulled from borosilicate capillaries with an ID of 0.78 mm using a Flaming-Brown P-97 micropipette puller (Sutter Instruments). For mass spectrometry analysis, 3−5 μL of sample was loaded into an emitter, and electrospray was initiated by applying a potential (relative to instrument ground) of +0.8−1.2 kV to a platinum wire in electrical contact with the solution. For native IM-MS experiments, the ion source temperature was equilibrated to ambient temperature, and for denatured and supercharging experiments, the source temperature was 150 °C. Mass spectra for the BSA and β-lactoglobulin reduction experiments were collected in "Resolution" mode, and all other mass spectra were collected in "Sensitivity" mode. The Trap and Transfer collision voltages were 5−15 and 5 V, respectively, and argon trap gas was used at a flow rate of 5−10 mL/min. The maximum charge state for which the signal-to-noise ratio was greater than 2:1 was determined to be the highest-observed charge state.

Traveling-wave ion mobility data were calibrated using an established procedure.[36,37] Cytochrome C, β-lactoglobulin, avidin, BSA, and concanavalin A were used as calibrants for native IM-MS analyses, and denatured (48/48/2 v/v/v water/methanol/formic acid) ubiquitin, cytochrome C, and myoglobin were used as calibrants for supercharged and denatured IM-MS analyses. Nitrogen was used as the buffer gas for ion mobility spectrometry at a flow rate of 50 mL/min. The traveling wave velocity was set to 450−600 m/s and the wave height to 10−20 V.

Gas-Phase Basicity Measurements. Ion−molecule reaction experiments were conducted at UNSW, Sydney, on a linear quadrupole ion trap mass spectrometer (LTQ-MS; ThermoFisher Scientific), modified with an ion funnel (Heartland Mobility) that is equipped with an external nanoelectrospray ionization (ESI) source. NanoESI emitter tips were prepared by pulling borosilicate capillaries (1.2 mm OD, 0.69 mm ID, Harvard Apparatus Limited) to an inner diameter of ~2 μm using a micropipette puller (Narishige PN-3, Narishige Scientific Instrument Laboratories) and sputter coated with a thin layer of Au and Pd for 20 s using a Scancoat Six (Edwards; Au/Pd alloy target). ESI emitters were positioned ~1−2 mm on axis from the heated capillary entrance to the MS. To establish ESI, a voltage of 1.0−1.9 kV was applied between the nanoESI emitter and heated capillary entrance. ESI solutions contained 10 μM of protein (either Ubq_1 or Ubq_3), 1/5/42/42 v/v/v/v acetic acid/BC/water/methanol. Protein charge states were isolated using an isolation window of ~±5 m/z that was centered on the ion of interest. Ion-molecule reaction times between size-selected protonated protein ions and neutral molecules (propane, water, methanol, hexamine, 3-fluoropyridine, pyridine, tri-*n*-propylamine) were varied between 0 and 30 s. Neutral molecules were introduced into the ion trap of the mass spectrometer through the standard He line that is modified with a custom gas mixer, which introduces the neutral molecule into the gas line as a vapor.[54,55] The effective temperatures of ions trapped by this type of mass spectrometer have been measured to be near ambient temperature.[56]

The bracketing method was used to determine the apparent gas-phase basicity (GB^{app}, which is the sum of $-\Delta G$ for the addition of a single proton to the ion at 298 K and the repulsive Coulomb barrier) of protein ions by observing proton transfer reactions between protein ions that have an unknown GB^{app} value with bases that have known gas-phase basicity values.[57,58] If proton transfer reactions are observed between the $[\text{protein}, (z+1)\text{H}]^{(z+1)+}$ and the base, this indicates that the GB^{app} of $[\text{protein}, z\text{H}]^{z+}$ is lower than the base. If the proton transfer reaction is not observed, the GB^{app} value of the corresponding protein ion is higher than the GB value of the neutral molecule. By use of a series of bases corresponding to a "ladder" of different GB values, GB^{app} values for an unknown ion can be assigned to within 10 kJ/mol.

The rates of proton transfer reactions between protonated protein ions and neutral molecules were calculated by fitting pseudo-first order rates of reaction to the precursor ion decay given by

$$-kt = \ln\left(\frac{I_0}{\sum I_i}\right)$$

where k is the rate constant of the reaction, t is the time in seconds, I_0 is the peak area of the isolated charge state, $\sum I_i$ is the sum of the peak areas of all the product ions. Proton-transfer rate constants were obtained from the linear regression best fits to plots of $\ln(I_0/\sum I_i)$ versus reaction time for a minimum of eight different reaction times. For all kinetic plots used to obtain the rate constants given in Table S-3, the R^2 values and y-axis intercepts were greater than 0.97 and near zero, respectively. Reaction rates less than 1.0×10^{11} cm^3 /mol·s were considered to be unreactive for the purposes of obtaining GB^{app} values.[57,58]

Circular Dichroism Spectroscopy. Circular dichroism (CD) spectra were acquired using a Jasco J-815 CD spectrometer. The spectral window for the experiments with Ubq_1 and Ubq_4 was 175−300 nm, and it was 200−260 nm for the experiments with BSA and β-lactoglobulin. CD spectra for all samples were corrected with a solvent blank.

Charge State and Collisional Cross Section Modeling. Linear straight-chain (φ = 180°, ψ = 180°) and α-helical (φ =

$-60°$, $\psi = -40°$) model structures of Ubq_{1-11} were constructed in Avogadro.[59] Optimal charge site configurations for the highest-observed charge states of supercharged Ubq_{1-11} were computed assuming either linear straight-chain or α-helical structure using Collidoscope[60] with proton affinities ($-\Delta H$ for the addition of a single proton to the residue at 298 K) or gas basicities of basic residues from literature values[61,62] and relative dielectric permittivity of 2.0. Corresponding collisional cross sections for linear straight-chain and α-helical $(Ubq_1)^{14+}$, $(Ubq_2)^{26+}$, and $(Ubq_3)^{37+}$ were computed by the Trajectory Method with N_2 as the buffer gas using Collidoscope.[60]

RESULTS AND DISCUSSION

Protein Structure in Native, Denaturing, and Supercharging Solution. Circular dichroism spectra of ubiquitin (Ubq_1) and tetra-ubiquitin (Ubq_4) in water, supercharging solution (94.5/5/0.5 water/BC/acetic acid), and denaturing solution (49/49/2 water/methanol/acetic acid) are shown in Figure 1. The CD spectrum of Ubq_1 in water is very similar to previously reported data for folded Ubq_1,[63] with a peak at 207 nm and a shoulder around 220 nm. Ubq_4 under the same solution conditions has a similar CD spectrum to Ubq_1, with an ellipticity approximately 2.6× that of Ubq_1, indicating that the secondary and tertiary structures of each Ubq monomer in Ubq_4 are similar to that of Ubq_1. The CD spectra of both proteins in supercharging solution are very similar to those in water, although for both proteins, there is a 5−10% decrease in signal at 207 nm and a 15−20% increase at 220 nm, indicating a small decrease in ordered secondary structure content. In contrast, the CD spectra in denaturing solution exhibit a marked increase in signal intensity at 207 and 220 nm compared to the spectra in water, consistent with a transition to the highly α-helical A state of Ubq_1, as previously reported for Ubq_1 in alcohol solutions.[63] The CD data indicate that Ubq_1 and Ubq_4 in supercharging solution have very similar secondary structure content to native, folded Ubq_1 and Ubq_4, and dramatically different secondary structure is observed for these proteins in denaturing solution.

Mass-Dependent Scaling Behavior of Charge State Distributions. In principle, proteins of different sizes can have different amino acid composition, potentially confounding accurate determination of charge-state or other scaling as a function of mass. To eliminate this potential confounding factor, mass spectra were acquired for head-to-tail linked polyubiquitins (Ubq_{1-11}) under native and supercharging conditions. The average (z_{avg}) and most abundant charge states for Ubq_{1-11} in native conditions and highest observed and most abundant charge states in supercharging conditions are shown in Table S-1. For native Ubq_{1-11} considered here, z_{avg} is found to scale as $(mass)^{0.55\pm0.01}$, in good agreement with previously reported values (0.54−0.57)[32,38−43] and slightly above that predicted for perfectly spherical, uniformly dense proteins based on the CRM (0.5; Figure 2a). The highest observed charge states for the supercharged Ubq_{1-11} scale according to a $(z-1)\times\ln(z-1)$ relationship (Figure 2b) and clearly do not follow a simple linear scaling law (Figure 2c). This scaling law ($mass \propto (z-1)\times\ln(z-1)$) was derived analytically (see Supporting Information) by treating the protein as a line segment with uniformly spaced point charges and assuming that the difference in the apparent gas-phase basicity[64] between the z_{max} and $z_{max}+1$ charge states is independent of protein size and is equal to the gas-phase basicity of water. This is supported by experimental gas-phase

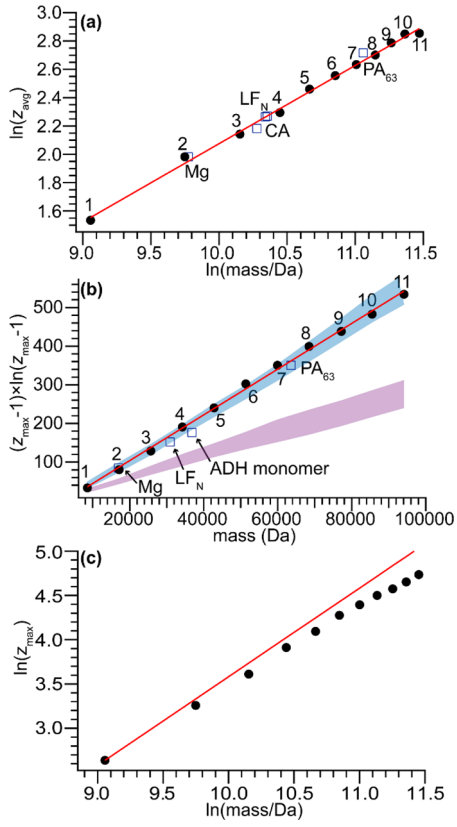

Figure 2. (a) Plot of $\ln(z_{avg})$ vs ln(mass) for native Ubq_{1-11} with linear trend line. (b) Plot of analytically derived scaling relation for highest observed charge states of supercharged Ubq_{1-11} vs mass, with linear trend line. The blue band is a range of calculated charge states for straight-chain Ubq_{1-11} using either gas-phase basicity (upper limit) or proton affinity (lower limit). The purple band is the same range for α-helical Ubq_{1-11}. (c) Plot of $\ln(z_{max})$ vs ln(mass) for supercharged Ubq_{1-11} with trend line showing hypothetical linear scaling that deviates significantly from observed data.

basicity measurements of supercharged Ubq_1 and Ubq_3, which are found to be 695.4 and 636.8 kJ/mol, respectively (Table S-3). These results indicate that Ubq_{1-11} ionized under native-like conditions have charge states consistent with the CRM for folded structures, and that supercharged Ubq_{1-11} adopt quasi-linear conformations during the electrospray process, consistent with the CEM and previous studies of Ubq_1.[46] Charge states for native-like or supercharged ions of all other proteins studied (myoglobin, carbonic anhydrase, alcohol dehydrogenase monomer, LF_N, and PA_{63}) agree well with these scaling laws, despite their different amino acid compositions (Table S-2), suggesting that amino acid composition is not the most important factor in the observed charge states for these ions.

Mass-Dependent Scaling of Collisional Cross Sections. IM-MS data were acquired for Ubq_{1-11} under native, denatured, and supercharging conditions. For native Ubq_{1-11}, the CCS of the most abundant charge state scales as $(mass)^{0.62\pm0.01}$ and that for the immediately lower charge state scales as $(mass)^{0.63\pm0.01}$, in good agreement with the expected two-thirds power scaling for folded, globular structures (Figure 3a). IM-MS data for myoglobin (17 kDa), LF_N (31 kDa), carbonic anhydrase (29 kDa), and PA_{63} (63 kDa) in native conditions follow a similar trend, with CCS values close to Ubq_{1-11} of similar mass. By contrast, for supercharged Ubq_{1-11}, the mass scaling powers for the CCSs of the highest and most

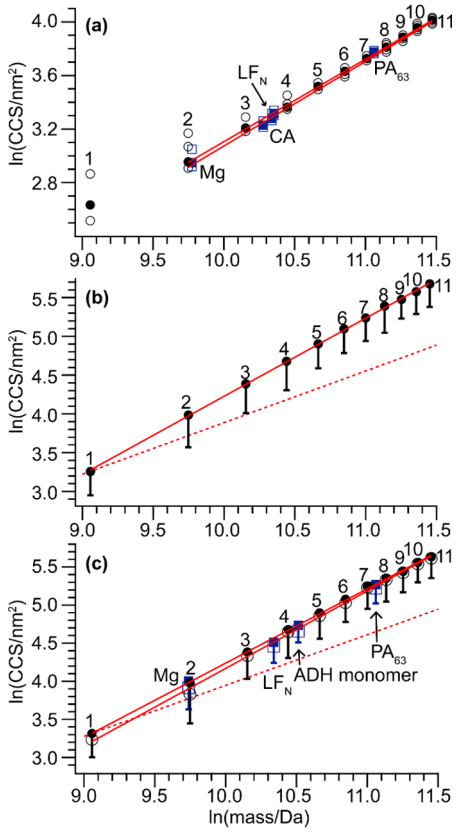

Figure 3. Plots of ln(CCS) vs ln(mass) for (a) native, (b) denatured, and (c) supercharged Ubq_{1-11} and other proteins (see text) with linear trend lines (solid). In (a), the most abundant charge state of Ubq_{1-11} (respectively, other proteins) is plotted as filled circles (respectively, squares) and other charge states as open circles (respectively, squares). Note that Ubq_1 falls below the size range used for IM calibration and thus was omitted from the fit. In (b) and (c), the highest observed charge state for Ubq_{1-11} (respectively, other proteins) is plotted as filled circles (respectively, squares), the most abundant charge state as open circles (respectively, squares), and the other charge states are represented by lines spanning the highest and lowest charge states. Hypothetical two-thirds scaling power trend lines are shown as dashed lines.

abundant charge states are 0.98 ± 0.01 and 1.02 ± 0.02, respectively (Figure 3c). Data for myoglobin, LF_N, alcohol dehydrogenase, and PA_{63} follow the same trend, with CCS values close to those of Ubq_{1-11} of similar mass. Thus, CCS scales linearly with mass for these supercharged, highly unfolded protein ions independent of the identity of the protein. For denatured Ubq_{1-11} ions, the CCS also scales linearly with mass (Figure 3b), with an experimental scaling power of 1.01 ± 0.01. Supercharging of these proteins creates ions with densities similar to those formed by nanoESI of solution-denatured proteins. The linear scaling of CCS with mass for both types of ions indicates that they have quasi-one-dimensional structures.

"Quasi-Linear" Structures. CCSs were computed for straight chain and α-helical Ubq_{1-3} (Figure S-1). Both structures exhibit linear CCS scaling, but CCS increases much more quickly with mass for straight chain Ubq_{1-3} (i.e., the slope of CCS vs mass is greater; Figure S-1). Experimental CCSs for Ubq_{1-3} are significantly greater than those calculated for α-helical structures and close to the straight chain values. This agrees with prior investigations of the structures of high charge states of ubiquitin and α-synuclein, which found that these ions are in highly unfolded conformations but are not completely linear chains; their CCS values approach but do not reach those calculated for a theoretical linear chain conformation.[46,65,66] Charge site calculations for Ubq_{1-11} demonstrate that the experimentally observed charge states fall much closer to those calculated for the straight-chain structures than for the α-helical structures (Figure 2b). These data support experimental structures that are significantly more unfolded than α-helical structures but are not completely straight chains. Interestingly, Ubq_{11} modeled as a straight chain (respectively, α-helix) is predicted to have a length of 300 nm (respectively, 126 nm), based on simple model structures using constant dihedral angles. These values are considerably larger than the initial diameter of ESI droplets in our experiments, which we estimate to be at most 100 nm, based on the inner diameter of the ESI emitters used. Although the actual structures adopted in these experiments are not perfectly straight, even significantly more folded/compact structures than these should have diameters close to or larger than the initial ESI droplet, consistent with very dramatic unfolding of the initial folded structures during the supercharging ESI process.

Effects of Internal Disulfide Bonds. To elucidate when unfolding occurs during supercharging, that is, "early" via a CEM-like mechanism[21,47,50,51] or "late" via a CRM-like mechanism,[52] a comparison of the extent of supercharging was performed for native and reduced BSA, β-lactoglobulin, and lysozyme, which contain 17, 2, and 4 disulfide bonds in their native forms. If protein unfolding occurs in the gas phase after charging by the CRM-like mechanism described by Konermann,[52] then the presence of internal disulfide bonds, which do not significantly affect folding in solution (see below), should have little effect on the observed charge states. However, if unfolding occurs in the droplet prior to or simultaneously with charging, as in the CEM, internal disulfides would be expected to decrease the amount of charging because they limit how extended the structure of the protein can become.

Reduced BSA, β-lactoglobulin, and lysozyme were buffer exchanged into ammonium acetate and the reduced and unreduced proteins were compared. CD spectroscopy of BSA and β-lactoglobulin shows that minor changes in secondary structure content occur following reduction. Unreduced BSA exhibits two peaks, one at 222 nm and another at 210 nm, characteristic of a structure rich in α-helical content and consistent with its crystal structure (Figure S-2d). A similar CD spectrum is observed for reduced BSA, albeit with a decrease in signal, indicating a small decrease in the amount of α-helix present and an increase in the amount of conformational flexibility, as expected for a compact structure with reduced disulfide bonds. The CD spectrum of unreduced β-lactoglobulin has a prominent peak at 218 nm and a shoulder at 208 nm, corresponding to a primarily β-sheet structure with a small amount of α-helical content (Figure S-3d). The CD spectrum of reduced β-lactoglobulin exhibits a 3% decrease in signal at 218 nm and a 9% increase at 208 nm, indicative of an increase in α-helical content and a slight shift toward a more disordered state, consistent with a largely folded protein with broken disulfide bonds.[67] However, the small magnitude of the changes indicates that reduced β-lactoglobulin remains in a similar conformation to the unreduced form.

For all three proteins, comparison of IM-MS data for the reduced and unreduced protein shows that following exchange into native ESI buffer the reduced protein retains a compact

conformation, as evidenced by the low and narrow charge state distributions. For BSA and lysozyme, the charge state distributions are virtually identical for the reduced and unreduced forms (Figures S-2 and S-4), while for β-lactoglobulin a smaller population of dimers and a small amount of higher charge states are observed in the mass spectrum of the reduced protein (Figure S-3). Comparison of arrival time distributions shows that the unreduced and reduced proteins have similar CCSs, with a 0−2% increase in drift time for the reduced species (Table S-4), within the ~3% uncertainty of the measurement.[36] This slight expansion is attributed to increased conformational flexibility upon reduction of the disulfide bonds. The CD and IM-MS results indicate that reduced BSA, β-lactoglobulin, and lysozyme can still adopt compact, native-like conformations, albeit with minor changes in secondary structure. Additionally, CD of BSA in supercharging conditions shows that the unreduced and reduced samples have similar secondary structure content (Figure 4).

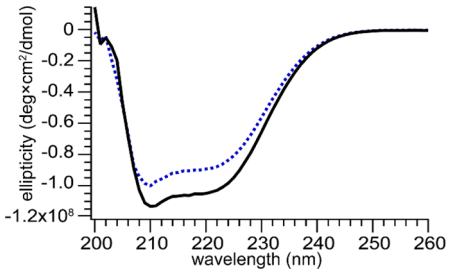

Figure 4. Circular dichroism spectra of unreduced (solid black line) and reduced (dashed blue line) BSA in supercharging solution.

However, compared to the CD spectra in native conditions, the peak at 210 nm is much more prominent. This is likely due to a conformational transition to the F state of BSA, in which domain II converts to a molten-globule state and the overall structure remains compact.[68−70]

Supercharging of reduced BSA, β-lactoglobulin, and lysozyme resulted in a marked increase in observed charge state as compared to the unreduced proteins. For BSA, the highest observed charge state increased from 78+ to 87+ and the most abundant charge state increased from 60+ to 70+ (Figure 5). For β-lactoglobulin, the highest observed charge state increased from 21+ to 23+, and the most abundant charge state of the reduced protein is 19+, while for the unreduced sample the charge state distribution is bimodal with local maxima at 15+ and 11+ (Figure S-5). For lysozyme, the highest observed charge state increased from 17+ to 19+ and the most abundant charge state increased from 11+ to 14+ (Figure S-5). Reduction of the internal disulfides thus leads to an increase in the charge state when supercharging, while both reduced and unreduced samples exhibit native-like, compact structures of very similar size when electrosprayed from buffered aqueous solution. Additionally, all of the reduced proteins access more unfolded conformations with larger CCS than the unreduced proteins across a range of charge states (Figure S-6). These data suggest that the ion charge states observed upon supercharging depend on the flexibility of the protein chain in solution and number of intact disulfide linkages, and not simply on the initial folded structure in solution. This strongly supports a supercharging mechanism for these ions whereby unfolding and ejection of these protein chains occurs during the

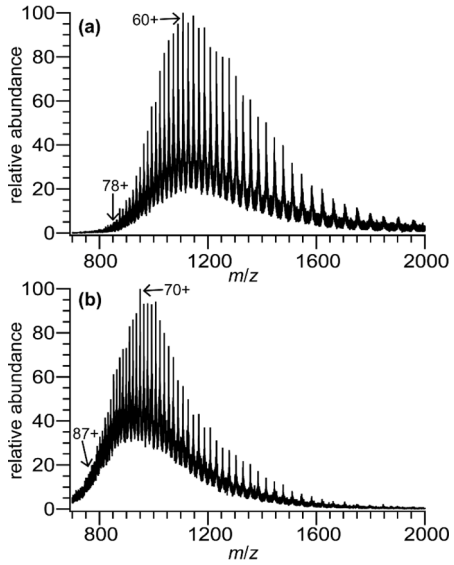

Figure 5. (a) Mass spectrum of supercharged, unreduced BSA. (b) Mass spectrum of supercharged, reduced BSA.

electrospray process and before all solvent and supercharging reagent have evaporated, that is, a CEM-like model.

CONCLUSIONS

IM-MS was used to systematically investigate the charge and CCS scaling behavior of supercharged proteins across a wide range of sizes and to investigate the mechanism of chemical supercharging in ESI. CD spectroscopy results confirm that Ubq_1 and Ubq_4 in supercharging solution have secondary structure content very similar to that of natively folded proteins and dissimilar to that of denatured Ubq_1 and Ubq_4. In contrast, IM-MS data for solution-denatured and supercharged proteins show that both charge state and CCS scale in a manner consistent with quasi-one-dimensional gas phase structures. We derive an analytical model that accurately predicts the experimental charge state behavior, and GB^{app} results verify the assumptions in the model. GB^{app} measurements also indicate that supercharged Ubq_1 and Ubq_3 are approximately as basic as water, so there is likely a quasi-equilibrium with water vapor that controls the extent of charging for highly unfolded protein ions. However, the GB^{app} of native-like Ubq_1 and Ubq_3 ions were found to be approximately the same as pyridine. These results agree with a recent report by Susa et al.[71] and suggest that charging of proteins via the CRM is limited by droplet size near the end of the evaporation process, whereas supercharging of proteins via the CEM occurs in the water-rich atmosphere of the electrospray plume and/or evaporating droplet at an earlier stage of evaporation. Reduction experiments show that the proteins with reduced disulfide bonds have structures similar to those with native disulfide bonds as demonstrated by native IM-MS and CD. However, the extent of charging increases for the reduced proteins in supercharging conditions, demonstrating that the amount of charging depends on the presence of internal disulfide bonds and not only on the overall folded structure. Those results are consistent with supercharging causing unfolding prior to evaporation of all solvent and suggests that supercharging proceeds by a CEM-like ionization mechanism rather than a CRM-like mechanism. We expect that systematic, simultaneous investigation of expected charge states and CCSs for model structures, such

as that described here, can lead to more accurate structure assignment with IM-MS and refinement of computational methods used to probe ionization dynamics.

■ ACKNOWLEDGMENTS

M.T.D. acknowledges support from a NSF GRFP (DGE-1309047). W.A.D. thanks the Australian Research Council for a Discovery Project (DP160102681). M.A.Z. thanks the Australian Department of Education and Training for an Australian Postgraduate Award. The authors thank Dr. Mike Harms for use of the Jasco J-815 CD spectrometer, Dr. Ryan Leib for helpful discussions, and Charlie Davis for running charge site calculations.

■ REFERENCES

(1) Benesch, J. L. P.; Ruotolo, B. T. *Curr. Opin. Struct. Biol.* **2011**, *21*, 641−649.
(2) Benesch, J. L. P.; Ruotolo, B. T.; Simmons, D. A.; Robinson, C. V. *Chem. Rev.* **2007**, *107*, 3544−3567.
(3) Baldwin, A. J.; Lioe, H.; Robinson, C. V.; Kay, L. E.; Benesch, J. L. P. *J. Mol. Biol.* **2011**, *413*, 297−309.
(4) Kintzer, A. F.; Thoren, K. L.; Sterling, H. J.; Dong, K. C.; Feld, G. K.; Tang, I. I.; Zhang, T. T.; Williams, E. R.; Berger, J. M.; Krantz, B. A. *J. Mol. Biol.* **2009**, *392*, 614−629.
(5) Uetrecht, C.; Versluis, C.; Watts, N. R.; Roos, W. H.; Wuite, G. J. L.; Wingfield, P. T.; Steven, A. C.; Heck, A. J. R. *Proc. Natl. Acad. Sci. U. S. A.* **2008**, *105*, 9216−9220.
(6) Xie, Y.; Zhang, J.; Yin, S.; Loo, J. A. *J. Am. Chem. Soc.* **2006**, *128*, 14432−14433.
(7) Loo, J. A. *Int. J. Mass Spectrom.* **2000**, *200*, 175−186.
(8) Robinson, C. V.; Chung, E. W.; Kragelund, B. B.; Knudsen, J.; Aplin, R. T.; Poulsen, F. M.; Dobson, C. M. *J. Am. Chem. Soc.* **1996**, *118*, 8646−8653.
(9) Loo, J. A.; Holsworth, D. D.; Root-Bernstein, R. S. *Biol. Mass Spectrom.* **1994**, *23*, 6−12.
(10) Uetrecht, C.; Barbu, I. M.; Shoemaker, G. K.; van Duijn, E.; Heck, A. J. R. *Nat. Chem.* **2011**, *3*, 126−132.
(11) Bleiholder, C.; Dupuis, N. F.; Wyttenbach, T.; Bowers, M. T. *Nat. Chem.* **2011**, *3*, 172−177.
(12) Scarff, C. A.; Thalassinos, K.; Hilton, G. R.; Scrivens, J. H. *Rapid Commun. Mass Spectrom.* **2008**, *22*, 3297−3304.
(13) Miladinović, S. M.; Fornelli, L.; Lu, Y.; Piech, K. M.; Girault, H. H.; Tsybin, Y. O. *Anal. Chem.* **2012**, *84*, 4647−4651.
(14) Meyer, J. G.; Komives, E. *J. Am. Soc. Mass Spectrom.* **2012**, *23*, 1390−1399.
(15) Sze, S. K.; Ge, Y.; Oh, H.; McLafferty, F. W. *Proc. Natl. Acad. Sci. U. S. A.* **2002**, *99*, 1774−1779.
(16) Bornschein, R. E.; Ruotolo, B. T. *Analyst* **2015**, *140*, 7020−7029.
(17) Hall, Z.; Politis, A.; Bush, M. F.; Smith, L. J.; Robinson, C. V. *J. Am. Chem. Soc.* **2012**, *134*, 3429−3438.
(18) Pagel, K.; Hyung, S.-J.; Ruotolo, B. T.; Robinson, C. V. *Anal. Chem.* **2010**, *82*, 5363−5372.
(19) Zhou, M.; Dagan, S.; Wysocki, V. H. *Analyst* **2013**, *138*, 1353−1362.
(20) Iavarone, A. T.; Williams, E. R. *J. Am. Chem. Soc.* **2003**, *125*, 2319−2327.
(21) Sterling, H. J.; Prell, J. S.; Cassou, C. A.; Williams, E. R. *J. Am. Soc. Mass Spectrom.* **2011**, *22*, 1178−1186.
(22) Lomeli, S. H.; Peng, I. X.; Yin, S.; Ogorzalek Loo, R. R.; Loo, J. A. *J. Am. Soc. Mass Spectrom.* **2010**, *21*, 127−131.
(23) Valeja, S. G.; Tipton, J. D.; Emmett, M. R.; Marshall, A. G. *Anal. Chem.* **2010**, *82*, 7515−7519.
(24) Verkerk, U. H.; Peschke, M.; Kebarle, P. *J. Mass Spectrom.* **2003**, *38*, 618−631.
(25) Lemaire, D.; Marie, G.; Serani, L.; Laprévote, O. *Anal. Chem.* **2001**, *73*, 1699−1706.
(26) Catalina, M. I.; van den Heuvel, R. H. H.; van Duijn, E.; Heck, A. J. R. *Chem. - Eur. J.* **2005**, *11*, 960−968.
(27) Sterling, H. J.; Cassou, C. A.; Susa, A. C.; Williams, E. R. *Anal. Chem.* **2012**, *84*, 3795−3801.
(28) Iribarne, J. V.; Thomson, B. A. *J. Chem. Phys.* **1976**, *64*, 2287−2294.
(29) Dole, M.; Mack, L. L.; Hines, R. L.; Mobley, R. C.; Ferguson, L. D.; Alice, M. B. *J. Chem. Phys.* **1968**, *49*, 2240−2249.
(30) Ahadi, E.; Konermann, L. *J. Phys. Chem. B* **2012**, *116*, 104−112.
(31) Konermann, L.; Rodriguez, A. D.; Liu, J. *Anal. Chem.* **2012**, *84*, 6798−6804.
(32) Fernandez de la Mora, J. *Anal. Chim. Acta* **2000**, *406*, 93−104.
(33) Yue, X.; Vahidi, S.; Konermann, L. *J. Am. Soc. Mass Spectrom.* **2014**, *25*, 1322−1331.
(34) Kebarle, P.; Verkerk, U. H. *Mass Spectrom. Rev.* **2009**, *28*, 898−917.
(35) Marklund, E. G.; Degiacomi, M. T.; Robinson, C. V.; Baldwin, A. J.; Benesch, J. L. P. *Structure* **2015**, *23*, 791−799.
(36) Bush, M. F.; Hall, Z.; Giles, K.; Hoyes, J.; Robinson, C. V.; Ruotolo, B. T. *Anal. Chem.* **2010**, *82*, 9557−9565.
(37) Ruotolo, B. T.; Benesch, J. L. P.; Sandercock, A. M.; Hyung, S.-J.; Robinson, C. V. *Nat. Protoc.* **2008**, *3*, 1139−1152.
(38) Testa, L.; Brocca, S.; Grandori, R. *Anal. Chem.* **2011**, *83*, 6459−6463.
(39) Testa, L.; Brocca, S.; Santambrogio, C.; D'Urzo, A.; Habchi, J.; Longhi, S.; Uversky, V. N.; Grandori, R. *Intrinsically Disord. Proteins* **2013**, *1*, e25068.
(40) Kaltashov, I. A.; Mohimen, A. *Anal. Chem.* **2005**, *77*, 5370−5379.
(41) Nesatyy, V. J.; Suter, M. J. F. *J. Mass Spectrom.* **2004**, *39*, 93−97.
(42) Heck, A. J. R.; van den Heuvel, R. H. H. *Mass Spectrom. Rev.* **2004**, *23*, 368−389.
(43) Tolić, L. P.; Anderson, G. A.; Smith, R. D.; Brothers, H. M.; Spindler, R.; Tomalia, D. A. *Int. J. Mass Spectrom. Ion Processes* **1997**, *165*, 405−418.
(44) Zenaidee, M. A.; Donald, W. A. *Analyst* **2015**, *140*, 1894−1905.
(45) Teo, C. A.; Donald, W. A. *Anal. Chem.* **2014**, *86*, 4455−4462.
(46) Going, C. C.; Williams, E. R. *Anal. Chem.* **2015**, *87*, 3973−3980.
(47) Sterling, H. J.; Kintzer, A. F.; Feld, G. K.; Cassou, C. A.; Krantz, B. A.; Williams, E. R. *J. Am. Soc. Mass Spectrom.* **2012**, *23*, 191−200.
(48) Cassou, C. A.; Williams, E. R. *Analyst* **2014**, *139*, 4810−4819.
(49) Sterling, H. J.; Williams, E. R. *Anal. Chem.* **2010**, *82*, 9050−9057.

(50) Sterling, H. J.; Daly, M. P.; Feld, G. K.; Thoren, K. L.; Kintzer, A. F.; Krantz, B. A.; Williams, E. R. *J. Am. Soc. Mass Spectrom.* **2010**, *21*, 1762−1774.
(51) Sterling, H. J.; Williams, E. R. *J. Am. Soc. Mass Spectrom.* **2009**, *20*, 1933−1943.
(52) Metwally, H.; McAllister, R. G.; Popa, V.; Konermann, L. *Anal. Chem.* **2016**, *88*, 5345−5354.
(53) Ogorzalek Loo, R. R.; Lakshmanan, R.; Loo, J. A. *J. Am. Soc. Mass Spectrom.* **2014**, *25*, 1675−1693.
(54) Donald, W. A.; McKenzie, C. J.; O'Hair, R. A. *Angew. Chem., Int. Ed.* **2011**, *50*, 8379−8383.
(55) Donald, W. A.; O'Hair, R. A. *Dalton Trans.* **2012**, *41*, 3185−3193.
(56) Donald, W. A.; Khairallah, G. N.; O'Hair, R. A. *J. Am. Soc. Mass Spectrom.* **2013**, *24*, 811−815.
(57) Schnier, P. D.; Gross, D. S.; Williams, E. R. *J. Am. Chem. Soc.* **1995**, *117*, 6747−6757.
(58) Williams, E. R. *J. Mass Spectrom.* **1996**, *31*, 831.
(59) Hanwell, M. D.; Curtis, D. E.; Lonie, D. C.; Vandermeersch, T.; Zurek, E.; Hutchison, G. R. *J. Cheminf.* **2012**, *4*, 17.
(60) Ewing, S. A.; Donor, M. T.; Wilson, J. W.; Prell, J. S. *J. Am. Soc. Mass Spectrom.* **2017**, *28*, 587−596.
(61) Marchese, R.; Grandori, R.; Carloni, P.; Raugei, S. *PLoS Comput. Biol.* **2010**, *6*, e1000775.
(62) Popa, V.; Trecroce, D. A.; McAllister, R. G.; Konermann, L. *J. Phys. Chem. B* **2016**, *120*, 5114−5124.
(63) Wilkinson, K. D.; Mayer, A. N. *Arch. Biochem. Biophys.* **1986**, *250*, 390−399.
(64) Schnier, P. D.; Gross, D. S.; Williams, E. R. *J. Am. Soc. Mass Spectrom.* **1995**, *6*, 1086−1097.
(65) Beveridge, R.; Chappuis, Q.; Macphee, C.; Barran, P. *Analyst* **2013**, *138*, 32−42.
(66) Wyttenbach, T.; Bowers, M. T. *J. Phys. Chem. B* **2011**, *115*, 12266−12275.
(67) Qi, X. L.; Holt, C.; McNulty, D.; Clarke, D. T.; Brownlow, S.; Jones, G. R. *Biochem. J.* **1997**, *324*, 341−346.
(68) Suzukida, M.; Le, H. P.; Shahid, F.; McPherson, R. A.; Birnbaum, E. R.; Darnall, D. W. *Biochemistry* **1983**, *22*, 2415−2420.
(69) El Kadi, N.; Taulier, N.; Le Huérou, J. Y.; Gindre, M.; Urbach, W.; Nwigwe, I.; Kahn, P. C.; Waks, M. *Biophys. J.* **2006**, *91*, 3397−3404.
(70) Dockal, M.; Carter, D. C.; Rüker, F. *J. Biol. Chem.* **2000**, *275*, 3042−3050.
(71) Susa, A. C.; Xia, Z.; Tang, H. Y. H.; Tainer, J. A.; Williams, E. R. *J. Am. Soc. Mass Spectrom.* **2017**, *28*, 332−340.